ELSEVIER

Catalysis Today 53 (1999) 419–432

CATALYSIS TODAY

www.elsevier.com/locate/cattod

Characterization of catalytically active sulfated zirconia

David J. Zalewski [a,*], Saeed Alerasool [b], Patricia K. Doolin [a]

[a] *Marathon Ashland Petroleum LLC, P.O. Box 911, Catlettsburg, KY 41129, USA*

[b] *Engelhard Corporation, 23800 Mercantile Road, Beachwood, OH 44122, USA*

Abstract

Catalytic activity of sulfated zirconia was affected by both sulfur loading level and surface crystal phase. Incorporating silica or alumina into the catalyst system stabilized the tetragonal crystal phase and prolonged activity. Stabilized sulfated zirconia prepared with 20 wt.% alumina maintained catalytic activity for the isoparaffin alkylation reaction six times longer than pure sulfated zirconia. This performance enhancement has, thus far, not been disclosed in the literature. Reasons for the enhanced performance are hypothesized.

UV–Raman spectroscopy was used to characterize the surface structure of sulfated zirconia. Samples displaying tetragonal reflections were catalytically active, while those displaying a surface monoclinic phase showed little activity. Examination of fresh, spent, and regenerated catalyst did not reveal any evidence for a phase transformation, indicating catalyst deactivation was most likely caused by the accumulation of hydrocarbon fragments on the surface.

1. Introduction

Sulfated metal oxides have gained attention due to their unusual ability to initiate acid catalyzed reactions at low temperatures [1,2]. Sulfated zirconia (SZr) can catalyze the following reactions: paraffin isomerization, paraffin cracking, isoparaffin alkylation, and acylation of aromatics [3–6]. Although SZr displays good initial activity, it quickly deactivates. The high initial activity is attributed to the unusual acidic characteristics of SZr. Despite numerous studies, there is no universally accepted theory regarding the nature of the catalytically active sites and the method by which they deactivate. Some authors claim strong Lewis centers [7] are responsible for the high activity, while others believe the unusual activity is associated with Brønsted acid sites [8]. Several postulates have also been offered to explain the rapid catalyst deactivation. These include loss of sulfur, change in sulfur oxidation state, transformation of the crystal structure, and deposition of hydrocarbon fragments.

Preparation conditions, such as precursor type, sulfur content, and activation temperature, are all known to influence the catalyst's crystal structure and activity [9–13]. Small variations in preparation conditions can dramatically alter the final catalytic properties [2]. This can help explain why the literature is filled with conflicting claims.

Zirconia samples are typically prepared from zirconium hydroxide precursors [1]. As the sample is calcined, Zr–OH groups condense to form the Zr–O–Zr lattice [2]. The final crystal phase depends on the sample history and calcination temperature. Upon thermal treatment, amorphous zirconia is first transformed into a metastable tetragonal phase. With increasing thermal treatment, the tetragonal phase is converted into the thermodynamically favored monoclinic phase. Formation of metastable tetragonal zirconia has been ratio-

* Corresponding author.

0920-5861/99/$ – see front matter
PII: S0920-5861(99)00137-6

nalized on the basis of surface strain energy effects [14,15]. Crystallites smaller than 100 Å are expected to form tetragonal zirconia. As the crystallites grow in size, the monoclinic phase becomes the dominate phase [16].

When amorphous zirconium hydroxide is treated with sulfate groups, the crystallization process is retarded [17]. Under identical calcination conditions, sulfated samples display a smaller crystallite size and increased amounts of tetragonal phase, relative to the corresponding non-sulfated material. Sulfate groups may act to relieve surface strain energy, thereby stabilizing the tetragonal phase, or they may prevent the crystallite size from growing to the critical diameter necessary to favor the monoclinic phase. In this study, we examined properties of both catalytically active and inactive samples. Comparisons were made between catalyst samples prepared from the same initial precursor. In this way, differences in the synthetic procedure are minimized. Sulfur loading level, activation temperature, catalyst support interactions, bulk and surface crystal phases were characterized. Catalyst formulations containing 20 wt.% silica or alumina were found to have increased tetragonal character and prolonged catalytic activity.

2. Experimental

2.1. Catalyst preparations

Zirconium hydroxide was precipitated by the dropwise addition of aqueous ammonia to zirconyl chloride. The product was collected by filtration and washed with distilled water until free of chloride ions. After washing, the sample was dried overnight at 100°C. Alternatively, zirconium hydroxide was supplied by Magnesium Elektron.

Sulfating was accomplished by treating the zirconium hydroxide sample with 1 N sulfuric acid. Zirconium hydroxide was slurred in a minimum amount of distilled water, followed by the dropwise addition of a sulfuric acid solution until the desired sulfate level was reached. The mixture was stirred for 1 h before excess water was removed by evaporation followed by overnight drying at 100°C. Samples were then placed in a muffle furnace and heated (10°C/min) in air to the final calcination temperature. The final temperature was maintained for 3 h before cooling the samples. Catalyst samples are abbreviated as follows: SZr (400) where the number in parenthesis represents the final calcination temperature in °C. Sulfated zirconium hydroxide obtained from Magnesium Elektron followed the calcination procedure outlined above.

Stabilized catalysts were prepared by mixing uncalcined SZr (100) with a phase stabilizer in distilled water. Additives used in this study were Silica Gel (Davison Chemical) or Catapol Alumina (Akzo). After stirring the slurry for 1 h, excess water was removed by evaporation followed by air drying at 100°C overnight. The material was then calcined in air at 600°C for 3 h {SZr/Si (600) or SZr/Al (600)}. Enhanced catalytic activity was only obtained when both precursors (SZr and stabilizer) were uncalcined. This would indicate mixed oxide formation occurs.

2.2. Catalyst characterization

Chemical analyses were obtained on a Phillips PW 1480 XRF after lithium tetraborate fusion. XRD analyses were performed on a standard Phillips XRG 3100. Nitrogen BET surface areas were measured on a Quantachrome Autosorb-6.

2.3. Acidity measurements

The number of acid sites was determined from thermogravimetric analysis (TGA) of pyridine adsorption [18]. Approximately 75 mg of sample were placed in the aluminum pan of a DuPont 951 TGA. The sample was heated at 10°C/min under a nitrogen purge to a final calcination temperature (400–600°C) and held for 2 h. After cooling to 150°C, the sample was exposed to pyridine by diverting the carrier gas through a pyridine saturator. After 1 h, a constant sample weight was observed. The sample was then purged with nitrogen to remove physisorbed pyridine. It took a minimum of 5 h to reach a constant weight. Total acidity (TA) was determined from the weight gain and expressed as micromole of acidity per gram of sample. Pyridine is a strong base that readily adsorbs on both weak and strong acid sites. Acidity values calculated from pyridine adsorption include both catalytically active and inactive sites.

Table 1
Hexane strength index and Hammett acidities of selected solid acids

Solid acid	Hexane strength index	$-H_0$
Silica–alumina HY	0.5–2.0	8.0–9.0
Dealuminated Y-zeolites CeY	1.0–5.0	9.0–11.0
USY, SZr	5.0–8.0	11.0–12.0
Mordenite	>8	>12

2.4. Hexane cracking activity

Hexane cracking was used to probe the relative acid strength and catalytic activity of the catalyst samples. Experiments were performed with 2.0 g of catalyst in a quartz microreactor. Sample activation was accomplished by purging the reactor with helium at 400°C for 2 h. Diverting the carrier gas through a saturator filled with *n*-hexane started the reaction. The saturator was held at 0°C to maintain a constant vapor pressure. After 5 min on stream, a pulse of the reaction products was sent to a gas chromatograph equipped with a flame ionization detector and Porapak N column. Activity was calculated and expressed in terms of [micromole hexane reacted]/[(gram catalyst) (hour)] [19]. By analyzing the reaction products after a time-on-stream of only 5 min the initial catalyst activity can be estimated. Relative acid strength was determined by dividing the initial activity by the total number of acid sites determined by pyridine adsorption. The value obtained in this manner is referred to as the 'hexane strength index' (SI) of the catalyst. The SI represents the average activity of individual acid sites on the catalyst surface. Although catalyst generally contain a distribution of acid strengths, the calculated SI value is useful for monitoring relative changes in acid strength. This is especially true when comparing catalyst systems that possess a similar acid site distribution. Table 1 compares the hexane strength indexes of various solid acids to their Hammett numbers [20]. As expected, a good correlation between SI and Hammett acidity values are observed.

2.5. Diffuse reflectance infrared spectroscopy (DRIFTS)

DRIFTS was used to determine relative amounts of Brønsted and Lewis acid sites [21]. The DRIFTS cell (Harrick Scientific) was equipped with a heater and connected to a vacuum system. Temperature was monitored with a thermocouple placed in direct contact with the sample. Other modifications made to the cell and diffuse reflectance accessory were similar to those reported by Venter and Vannice [22]. Experiments were conducted on 100 mg of sample. A dry nitrogen purge was passed over the catalyst while it was heated to a final temperature of 400°C. The sample was maintained at 400°C for 2 h before being cooled to 40°C to collect the reference spectrum. The sample was reheated to 150°C prior to being saturated with pyridine. The sample chamber was purged with nitrogen for 2 h at 150°C to remove any physisorbed pyridine, then cooled to 40°C to record the sample spectrum. The sample was reheated to 350°C to remove weakly adsorbed pyridine. After recooling to 40°C, the final spectrum was recorded. Baseline corrections were performed on spectra before relative populations of Brønsted and Lewis acid sites were estimated from peak intensities of bands observed at 1542–1545 cm^{-1} (Brønsted) and 1148–1455 cm^{-1} (Lewis).

2.6. Alkylation reactions

Isoparaffin alkylation reactions were conducted in a 100 ml autoclave stirred tank reactor. Isobutane and 2-butene flows were controlled with an ISCO System D500 continuous syringe pump. The following reactor conditions were used: 350 psig, 28°C, olefin weight hourly space velocity (OWHSV) 0.20 h^{-1}, isoparaffin/olefin ratio of 52, 1200 rpm stirring.

Catalysts were pre-dried in air at 400°C for 6 h prior to loading into the reactor. It was then treated in situ at 400°C under a nitrogen purge for 6 h. After cooling the reactor to room temperature, it was pressurized to 350 psig with nitrogen and filled with isobutane. After establishing the desired isobutane flow, 2-butene was introduced into the reactor to initiate the reaction. Product analysis was accomplished with an on-line Hewlett–Packard Model 5890 gas chromatograph equipped with a flame ionization detector and a 150 m, 0.25 capillary column (Supelco Petrocal™ DH150 fused silica, 1.0 μm film thickness).

2.7. UV–Raman spectroscopy

UV–Raman spectra were collected in Professor Peter Stair's laboratory at Northwestern University. Catalyst samples were initially dried in a nitrogen purged oven at 400°C, pressed into discs, then placed into a quartz reactor cell where they were again pretreated in a nitrogen atmosphere. Spectra were collected using a 257.2 nm excitation source [23–25]. To avoid thermal decomposition, laser power was kept below 5 mW. Raman scattering from the sample was collected using a backscattering geometry by an $AlMgF_2$ coated ellipsoidal reflector, focused into a single grating spectrograph through a notch filter. A multi-channel photomultiplier tube was used as the detector. Slit widths between 100 and 200 μm were used.

3. Results and discussion

3.1. Impact of activation temperature on sulfated zirconia

To examine the effect of activation temperature, a large batch of sulfated zirconium hydroxide was prepared. The sulfur level of this precursor was controlled to produce a sample containing 4.3 wt.% sulfur after calcination at 300°C (SZr (300)). Calcination at 300°C was not sufficient to completely form the zirconium oxide lattice. Only a broad, poorly defined signal was observed in the XRD spectrum, indicative of low sample crystallinity. To follow changes that occur with the formation of the zirconia lattice, aliquots of the initial sulfated zirconium hydroxide sample was subjected to calcination temperatures between 300 and 700°C. By utilizing the same initial catalyst precursor, differences in synthetic parameters were eliminated.

SZr (300) had a surface area of 195 m^2/g and a sulfur loading level of 4.3 wt.%. Each sulfate ion occupies a surface area of 25 $Å^2$. Monolayer sulfate coverage corresponds to four sulfur atoms/nm^2 [26]. Assuming the sulfate groups are located on the surface, SZr (300) used in this study initially contained a monolayer coverage of sulfate groups (4.1 atoms/nm^2). Zirconium oxide contains eight surface zirconium atoms per square nanometer [27]. When a zirconium surface is saturated with sulfate ions, there are two Zr atoms for every sulfur atom. Sulfate groups can chelate to a single zirconium atom or form bridges between two or more zirconium centers [1,2]. Regardless of the coordination mode, the presence of sulfate ions retards the crystallization process and delays the tetragonal to monoclinic transformation.

As activation temperature increased, catalyst surface area was reduced, sulfur content was reduced, and sample crystallinity was increased (Table 2). These general trends are commonly observed on SZr systems, regardless of the preparation method [1,2]. The reduction in surface area lowers the number of sulfate groups required for monolayer coverage. Sulfate groups must dissociate from the surface or diffuse into the bulk lattice. Below activation temperatures of 600°C, the calculated sulfur density remained constant (Table 2), indicating sulfate groups were removed at a rate proportional to the loss in surface area. When the activation temperature was increased to 700°C, only strongly adsorbed sulfate groups remained attached to the surface and the calculated sulfur density dropped below monolayer coverage (1.8 atoms/nm^2).

Catalytic activity, as determined from the hexane cracking reaction, began after activation at 400°C. SZr (400) displayed the highest total acidity, along with a high acid strength index. XRD analysis of SZr (400) indicated the sample is mainly amorphous, but beginning to show signs of the tetragonal zirconia phase. Zirconia crystallites of SZr (400) may be too small to provide a good XRD pattern. Sample crystallinity increased with activation temperature. As this occurred, the total number of acid sites was reduced, while the hexane strength index displayed a modest increase.

3.2. Effect of sulfur loading level on SZr (400)

The effect of sulfur level on catalyst properties was examined by preparing catalysts with sulfur contents between 2.2 and 8.5 wt.% (Table 3). To minimize synthetic variables, samples were prepared from the same batch of zirconium hydroxide. The final sulfur level was controlled by altering the amount of 1 N sulfuric acid used to prepare the catalyst. A maximum in surface area and total acidity was observed at a sulfur loading level of 4.4 wt.% (3.6 atoms/nm^2).

Infrared spectra were collected after saturating the surface with pyridine (Fig. 1). At low sulfur concentrations (<3 atoms/nm^2), Lewis acid sites dominated

Table 2
Effect of activation temperature on the properties of sulfated zirconia catalyst

Activation temperature (°C)	Sulfur (%)	Surface area (m^2/g)	Total acidity (μmol/g)	Hexane strength index	Sulfur density (atoms/nm^2)
300	4.3	195	348	1.5	4.14
400	3.9	180	370	6.5	4.07
600	2.4	112	183	7.1	4.02
700	0.7	71	144	7.9	1.85

Table 3
Effect of sulfur level on sulfated zirconia catalyst calcined at 400°C

Sulfur (%)	Surface area (m^2/g)	Total acidity (μmol/g)	Hexane strength index	Sulfur density (atoms/nm^2)
0.0	162	252	0.0	0.0
2.2	145	332	0.5	2.85
4.4	227	427	6.3	3.64
8.5	42	126	0.0	38.01

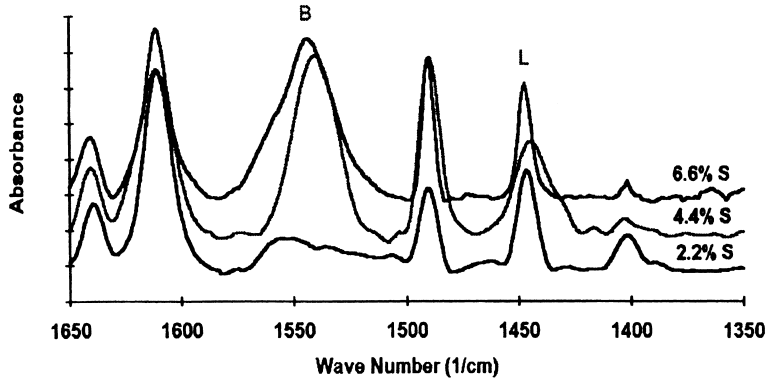

Fig. 1. DRIFTS spectra of sulfated zirconia calcined at 400°C {SZr (400)}.

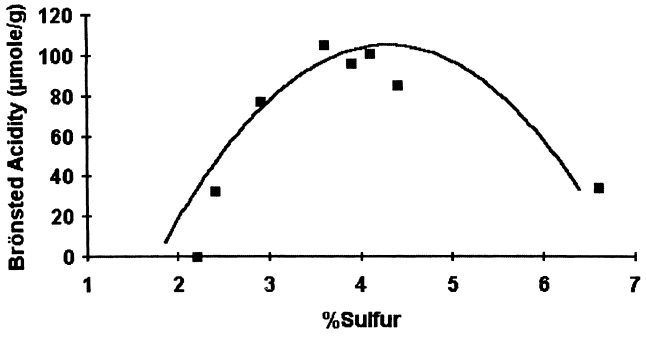

Fig. 2. Effect of sulfur content on the Brønsted acidity of sulfated zirconia catalyst calcined at 400°C.

the acidity profile. The concentration of Brønsted acid sites increased as the sulfate concentration approached monolayer coverage. Exceeding monolayer coverage resulted in a broadening of the Brønsted peak without significantly affecting its overall intensity. The total number of Brønsted acid sites reached a maximum at a sulfur loading level of 4 wt.% (Fig. 2), which corresponds to near monolayer coverage of 3.6 atoms/nm^2.

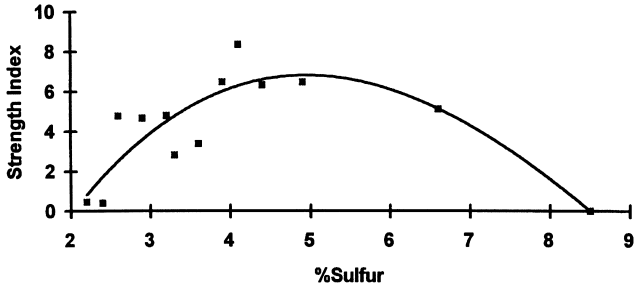

Fig. 3. Effect of sulfur content on the acid strength index of sulfated zirconia calcined at 400°C.

Table 4
Physical properties of SZr (600) catalysts containing alumina

Alumina (%)	Sulfur (%)	Surface area (m^2/g)	Total acidity (μmol/g)	Hexane strength index	Sulfur density (atoms/nm^2)
0	1.60	72	179	7.7	4.2
9	3.64	130	258	7.2	5.3
17	2.90	136	284	7.2	4.0
22	2.87	166	326	5.7	3.3
37	2.68	189	346	4.3	2.7
49	1.50	221	362	3.0	1.3
100	0.00	118	311	0.0	0.0

At higher sulfur loading, the total acidity and hexane cracking activity dropped off. Hexane cracking activity followed the Brønsted acidity, increasing until the sulfur level reached 4.4 wt.% (3.6 atoms/nm^2) (Fig. 3).

XRD patterns for sulfated zirconia samples calcined at 400°C are shown in Fig. 4. The sulfur free sample displayed reflections at 2θ equal to 30.3 and 50.3°C, consistent with tetragonal zirconia. Only traces of the monoclinic phase could be observed in the diffraction pattern. After adding 2.2 wt.% sulfur, the intensity of observed reflections was reduced. However, the tetragonal phase was still observed. The sample containing 4.4 wt.% sulfur appeared amorphous, with only broad ill-defined lines being observed in the XRD pattern. These results are in agreement with published reports where sulfur was found to inhibit the crystallization process [2,28].

3.3. Stabilized catalyst

Catalytic activity of SZr improved when it was combined with a high surface area material. Increased activity was obtained by incorporating either alumina or silica into the catalyst system prior to the final calcination. Improved activity was only obtained when the additives and SZr were mixed as hydroxides. This implies some mixed oxide formation occurs. After calcination at 600°C, silica and alumina displayed surface areas of 542 and 118 m^2/g, respectively. In comparison, the surface area of SZr (600) was only 72 m^2/g. Alumina contains weak acid sites (TA = 311 μmol/g) and displays a strong interaction with SZr, while silica is non-acidic (TA = 29 μmol/g) and only weakly interacts with SZr. Neither additive was capable of initiating hexane cracking or isoparaffin alkylation reaction.

SZr catalysts were prepared with up to 50% alumina (Table 4). Surface area and total acidity increases with alumina content, while the hexane strength index (SI) decreased. This is not surprising since alumina contributes weak acid sites that can not catalyze the hexane cracking reaction. Surface areas and total acidity values are both higher than predicted from the weighted average of the catalyst components. This indicates there is some beneficial interactions between alumina and zirconia. Maximum isoparaffin alkylation activity occurred on catalysts containing 20% alumina.

To compare the stabilizing effects of different supports, catalysts containing ~20 wt.% silica or alumina

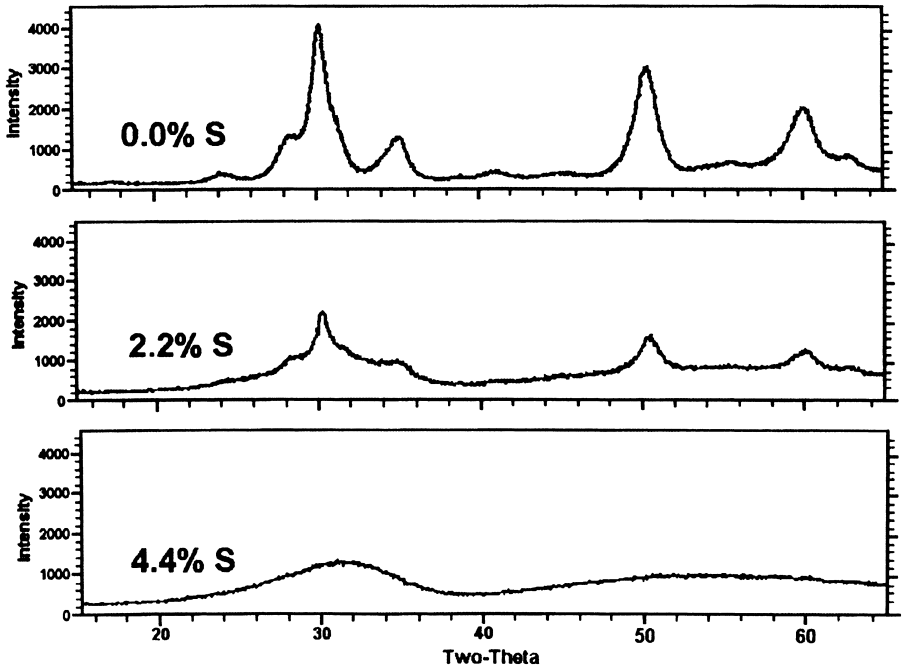

Fig. 4. Effect of sulfur concentration on the crystallinity of sulfated zirconia calcined at 400°C.

Table 5
Physical properties of supported catalysts

Catalyst	Sulfur (%)	Surface area (m^2/g)	Total acidity (μmol/g)	Hexane strength index	Sulfur density (atoms/nm^2)
SZr (600)	0.75	101	218	12.8	1.39
SZr/Si (600)	2.15	194	185	9.5	2.08
SZr/Al (600)	2.60	151	284	7.5	3.23

were prepared (Table 5). To minimize the differences between catalyst preparations, the same batch of SZr (100) was used to prepare the stabilized catalyst samples.

When silica was incorporated into the catalyst, the surface area increased, while a drop in total acidity and acid strength was observed. Since silica is non-acidic, a 20% drop in total acidity was expected. The weighted average acidity calculated from pure sulfated zirconia and pure silica predicts a total acidity of 177 μmol/g. This is close to the measured value of 185 μmol/g and would indicate no new acid sites are generated by any Si–O–Zr interactions. The surface area of SZr/Si (600) (194 m^2/g) was also close to the weighted average of the pure components (195 m^2/g). Hexane strength index dropped slightly, from 12.8 to 9.5, as silica was added to the catalyst. Silica does not contribute appreciable acidity to the system. All of the acid sites are associated with the SZr fraction of the catalyst. The SI of SZr/Si (600) should be comparable to pure SZr (600).

When alumina was used to stabilize the catalyst, both surface area and total acidity increased. Alumina contributes weak acid sites (311 μmol/g), and therefore would raise the total number of acid sites determined by pyridine adsorption. The average acid strength was found to decline as alumina was incorporated into the catalyst. This system contains a bi-modal distribution of acid sites. Weak acid sites should be present on the alumina phase, while strong acid sites should be located on the SZr portion of the catalyst. Calculating the total acidity of SZr/Al (600)

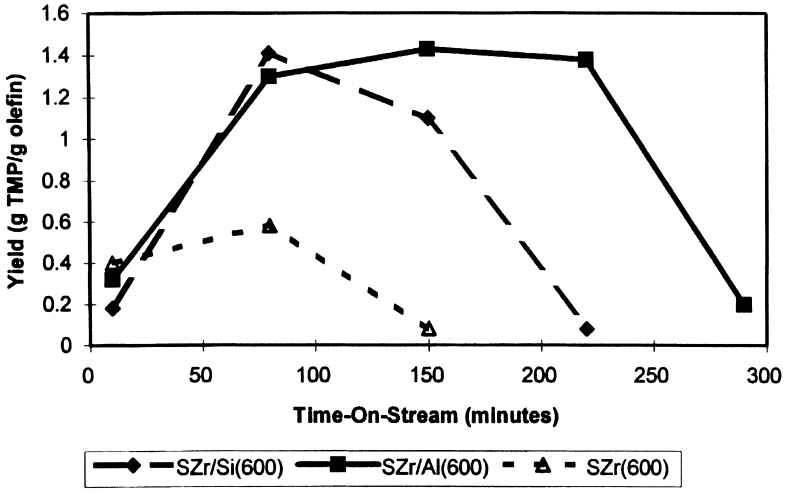

Fig. 5. Effect of high surface area supports on the trimethylpentane (TMP) yield obtained during the isoparaffin alkylation reactions.

based on the weighted average acidity of the precursors predicts a value of 237 μmol/g. This was significantly lower than the observed value (284 μmol/g), suggesting alumina interacts with SZr to generate new acid sites. Further evidence for this interaction comes from surface area measurements. The calculated surface area (104 m^2/g) was well below the measured value (151 m^2/g).

Fig. 5 compares the isoparaffin alkylation activity of supported and unsupported catalysts. Reaction conditions for the three runs were identical, with an isoparaffin/olefin ratio of 52 and an olefin weight hourly space velocity of 0.2. Addition of either silica or alumina to the catalyst system improved its activity. The activity of SZr (600) began to decline after only 40 min of reaction time. SZr/Si (600) and SZr/Al (600) maintained their peak activity for ≈133 and 220 min, respectively. The sample containing alumina {SZr/Al (600)} was able to maintain its peak catalytic activity approximately six times longer than pure SZr (600). The improved activity of the stabilized catalyst systems is remarkable, especially considering they contain 20 wt.% less of the active SZr component.

Since SZr/Si (600) is diluted with silica, it has a lower total acidity than the base SZr (600) catalyst, yet it can maintain catalytic activity longer than SZr. SZr/Si (600) has a higher surface area and increased sulfur density compared to SZr (600). SZr (600) had a sulfur density of only 1.4 S atoms/nm^2, or ≈35% of monolayer coverage. SZr/Si (600) displayed a sulfur density of 2.1 atoms/nm^2, or 53% of monolayer coverage. The most active catalyst, SZr/Al (600), displayed a sulfur density of 3.2 atoms/nm^2, which corresponds to 81% of monolayer coverage. If one assumes the sulfur is associated with zirconia rather than alumina, the sulfur coverage of SZr/Al (600) would approach monolayer coverage.

3.4. UV–Raman spectroscopy

Raman spectroscopy is based on the inelastic scattering of photons, which lose energy by exciting sample vibration modes. Raman spectroscopy is adaptable for in situ studies which makes it an ideal tool for studying catalytic systems. Catalyst supports such as silica and alumina are weak Raman scatters, therefore spectrum of adsorbed species can be recorded. A disadvantage of Raman spectroscopy is that many important catalytic samples display a fluorescence, which obscures the desired bands. Stair and co-workers have developed a technique that greatly reduces the surface fluorescence observed in Raman spectroscopy [23]. By utilizing ultra-violet (UV) excitation at 257 nm, Raman spectra of catalyst samples can be obtained [24,25]. Raman scattering occurs both at the surface and from the bulk of a sample. However, since the bulk signal is attenuated with depth, the recorded Raman spectrum is dominated by the outermost portion of the

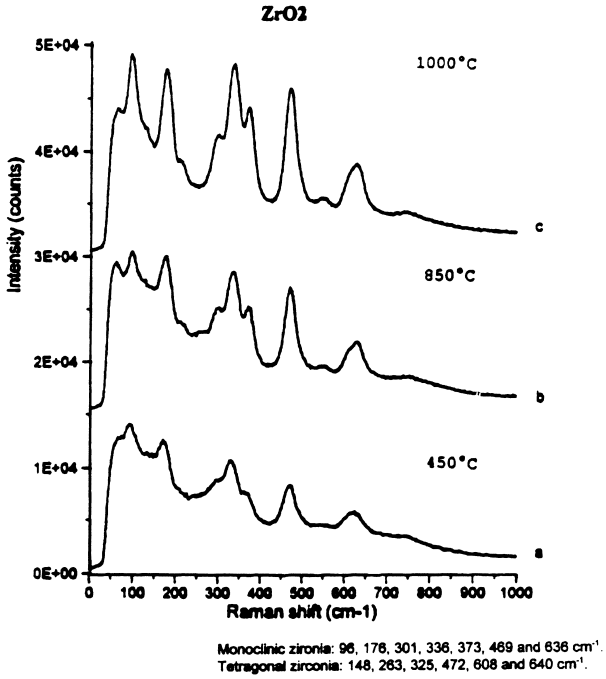

Fig. 6. UV–Raman spectra of zirconia oxide calcined at: (a) 450°C; (b) 850°C; and (c) 1000°C.

sample [23]. Metal oxide systems strongly adsorb UV light, which further enhances the surface sensitivity [23]. This feature is particularly useful when studying catalytic systems, since organic transformations occur on the outer most surface.

UV–Raman spectroscopy is useful in distinguishing the monoclinic and tetragonal phases of zirconia [23]. This is important since the catalytic activity of SZr has been related to its crystal phase [29,30]. Highly active catalysts are tetragonal in nature, while monoclinic samples generally display low activity [31].

Crystal structures of samples are generally determined by X-ray diffraction (XRD) analysis. XRD is a bulk technique that provides the average crystal environment. In contrast, UV–Raman offers the advantage of being more sensitive to the catalyst surface.

3.5. UV–Raman spectra of zirconium oxide

To aid in band assignments, UV–Raman spectra of pure zirconium oxide was examined. Samples were prepared by calcining zirconium hydroxide at 450, 850, and 1000°C. XRD analysis indicated the zirconia crystal phase changes from tetragonal to monoclinic as the calcination temperature increased [1,2]. Approximate crystallite sizes, calculated from XRD line widths, were also observed to increase with calcination temperature: 101 Å (450°C); 282 Å (850°C); and 440 Å (1000°C). Similar crystallite sizes were reported by Mercera et al [16].

Fig. 6 displays UV–Raman spectra of zirconium oxide samples. Spectral intensity increased with calcination temperature. This was expected since the Raman scattering increases with sample crystallinity. After calcination at 1000°C, Raman bands appear at 96, 176, 301, 336, 373, 469, and 636 cm^{-1}. This pattern matches that reported for monoclinic zirconia [16]. Tetragonal zirconia is expected to contain Raman bands at 148, 263, 325, 472, 608, and 640 cm^{-1} [16]. XRD analysis of Zr (1000) reveals a strong monoclinic pattern, which is consistent with the above Raman pattern. After calcination at 850°C, the XRD pattern contains reflections from both monoclinic and tetragonal zirconia. The intensity of the XRD patterns would suggest this sample contained approximately equal concentrations of tetragonal and monoclinic zirconia. In contrast to the XRD data, distinct tetragonal peaks were not observed in the UV–Raman spectrum

(Fig. 6). Instead, the UV–Raman pattern of Zr (850) closely matches that of the Zr (1000). After calcination at 450°C, the XRD pattern indicated tetragonal zirconia was the dominant phase. Once again the UV–Raman spectra showed significant adsorptions for monoclinic zirconia without any distinct bands for tetragonal zirconia.

Since Raman bands for monoclinic and tetragonal zirconia overlap, it is difficult to isolate the individual crystal phases. Stair and co-workers have used the relative peak intensities to characterize changes in the monoclinic/tetragonal ratio [25]. As calcination temperature is changed, the monoclinic/tetragonal peak intensities change. Our data suggests bands at 274, 340, and 469 cm^{-1} are especially sensitive to changes in the crystal structure. Raman bands at 340 and 469 cm^{-1} are present in both monoclinic and tetragonal zirconia, while the band at 274 cm^{-1} is unique to the tetragonal phase. Ratios of the 340/274 and 469/274 bands in the monoclinic sample {Zr (1000)} are 2.7 and 2.3, respectively. These values drop to 0.8 and 0.6 for a tetragonal sample. Using intensity ratios to calculate the amount of monoclinic phase present results in the following: Zr (1000) 100% monoclinic, Zr (850) 60% monoclinic, Zr (450) 34% monoclinic. This is in qualitative agreement with the XRD data; however, UV–Raman spectroscopy indicates a higher percentage of monoclinic phase than observed by XRD. This anomaly can be explained if surface structure of ZrO_2 is enriched in the monoclinic phase. XRD analysis provides the bulk crystal phase, while UV–Raman provides an indication of the surface structure.

3.6. UV–Raman spectra of SZr (600)

Two unsupported SZr (600) samples were examined via UV–Raman spectroscopy. These samples were prepared from the same zirconium hydroxide precursor. Using different amounts of 1 N sulfuric acid during the doping stage controlled final sulfur loading levels. The first sample was catalytically inactive for both hexane cracking and isoparaffin alkylation, while the second sample possessed good catalytic activity. Physical properties of these two materials are provided in Table 6.

Table 6
Characteristics of active and inactive SZr (600) catalyst

Description	Inactive	Active
Surface area (m^2/g)	5	122
N_2 pore volume (cc/g)	0.01	0.16
Average pore radius (Å)	46	26
Total acidity (μmol/g)	43	235
Hexane cracking activity	0.3	9.6
Hexane strength index	1.3	6.7
Sulfur content (wt.%)	3.95	2.77
Sulfur density (atoms/nm^2)	148	4.26
XRD pattern	Poor	Tetragonal monoclinic

The inactive sample possessed low total acidity and low surface area. XRD analysis revealed a broad, poorly resolved pattern. High sulfate concentrations inhibit zirconia crystallization [1,2], resulting in the poor diffraction pattern. In addition, sulfate groups appear to fill or block access to the pore structure, thereby leaving only the external surface area accessible. The UV–Raman spectrum was also featureless in the Zr–O stretching region (Fig. 7). However, a relatively strong adsorption band occurred between 950 and 1250 cm^{-1} (maximum at 1065 cm^{-1}). This corresponds to an S–O stretching vibration, and suggests the catalyst surface was saturated with sulfate groups. The surface area of this sample was only 5 m^2/g. Making the assumption that all of the sulfate groups were located at the catalyst surface, the sulfur density would be 148 atoms/nm^2, greatly exceeding monolayer coverage. Sulfur must be incorporated into sample bulk and/or trapped inside the catalyst pore structure. The present samples were calcined at 600°C for 3 h. This treatment would be expected to remove any physisorbed species located on the catalyst surface. In contrast to this, the active SZr (600) sample had a calculated sulfur density (4 atoms/nm^2) close to monolayer coverage.

The active sample displayed a good acidity profile with a total acidity of 235 μmol/g and a hexane strength index of 6.7. XRD analysis showed the sample to be tetragonal in nature, with only traces of monoclinic zirconia being detected. The UV–Raman band at 274 cm^{-1} (Fig. 2) indicated presence of tetragonal zirconia; however, the band at 340 cm^{-1} suggests the monoclinic phase is also present. The 340/274 and 470/274 intensity ratios are 1.4 and 1.3, respectively. This calculates to ≈35% monoclinic zirconia. The XRD pattern indicates the sample contains mainly tetragonal zirconia with only a trace of monoclinic

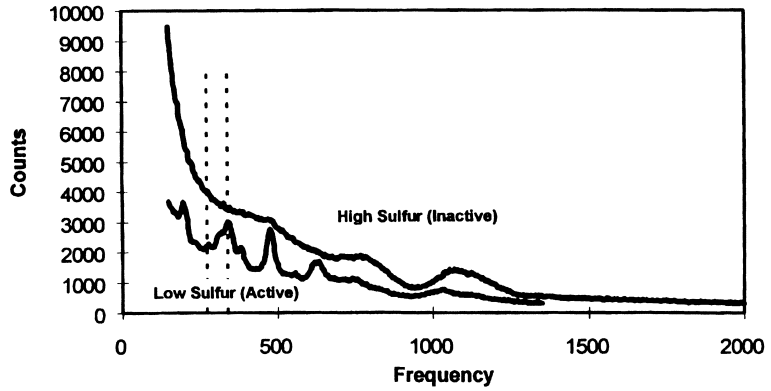

Fig. 7. UV–Raman spectra of unsupported sulfated zirconia catalysts {SZr (600)}. A comparison between a high sulfur (3.95 wt.%) inactive catalyst and a low sulfur (2.77 wt.%) active catalyst.

zirconia being present. As stated above, XRD analysis characterizes bulk properties, while UV–Raman is more selective toward the outer surface. The surface of SZr (600) appears to be enriched in the monoclinic phase, even though the bulk structure determined by XRD is tetragonal. An S–O stretching vibration was observed in the UV–Raman spectrum at 1023 cm^{-1}. Its intensity is much weaker than that observed for the inactive sample. This is consistent with the surface of the inactive sample being saturated with sulfate groups.

Neither sample displayed S=O stretching vibrations in the 1400 cm^{-1} region. The acid strength of SZr catalyst is related to the oxidation state of the promoting sulfur atom. The S–O and S=O stretches could provide valuable information on the structure of the sulfate group; unfortunately, these bands were not well resolved in the present samples. UV–Raman spectroscopy was not able to characterize the sulfur coordination mode.

3.7. UV–Raman spectra of stabilized sulfated zirconia catalyst

Catalytic activity of SZr was found to increase after being combined with alumina. UV–Raman spectroscopy was used to characterize the supported catalyst calcined at 600°C. Alumina supported samples were prepared with sulfur contents ranging from 2.3 to 9.9 wt.%. The stabilized samples were prepared from the same zirconium hydroxide precursor, with sulfur levels being controlled by the amount of 1 N sulfuric acid added. Physical properties of these catalysts are listed in Table 7.

Table 7
Characteristics of SZr/Al (600) catalyst[a]

Description	Low sulfur		High sulfur
Surface area (m^2/g)	161	55	6
N_2 pore volume (cc/g)	0.01	0.004	0.001
Average pore radius (Å)	17	16	45
Total acidity (μmol/g)	285	179	29
Hexane cracking activity	16.2	11.4	1.1
Hexane strength index	9.3	10.4	6.4
Sulfur content (wt.%)	2.3	5.3	9.9
Sulfur density (atoms/nm^2)	2.68	18.1	310
XRD pattern	Tetragonal	–	Poor

[a] All samples contain 20 wt.% alumina.

As the sulfur content increased, the surface area dropped from 161 to 6 m^2/g. The sample with 9.9 wt.% sulfur had a calculated sulfur density of 310 atoms/nm^2. This was similar to the unsupported SZr displaying multi-layer sulfate adsorption. The saturated sample gave rise to poor XRD and UV–Raman spectra. A weak tetragonal pattern was observed by XRD, while the UV–Raman spectrum was featureless in the Zr–O stretching region (Fig. 8). Two distinct bands were observed in the S–O stretching region. A broad band at 1070 cm^{-1} was similar to that observed on the unsupported sample. A second sharper band is seen at 1147 cm^{-1}. This band could result from sulfate groups trapped inside the catalyst pore structure, or from sulfate groups interacting with the alumina.

The XRD pattern obtained on the sample with 2.3 wt.% sulfur displayed strong tetragonal bands.

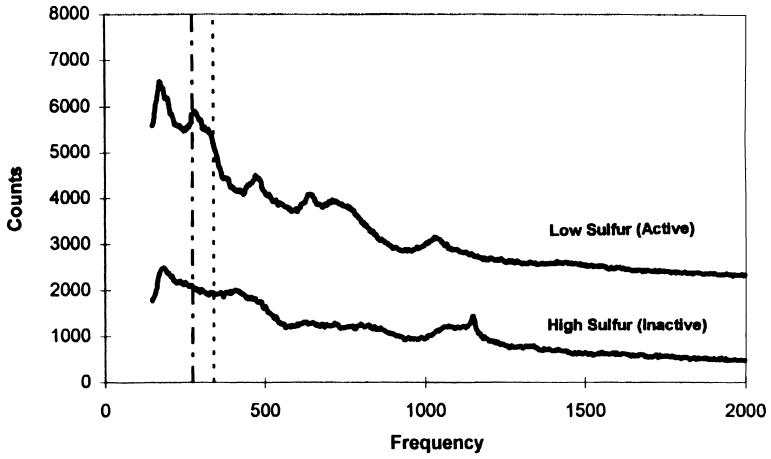

Fig. 8. UV–Raman spectra of alumina supported sulfated zirconia catalyst {SZr/Al (600)}. A comparison between active low sulfur (2.3 wt.%) and inactive high sulfur (9.9 wt.%) catalysts.

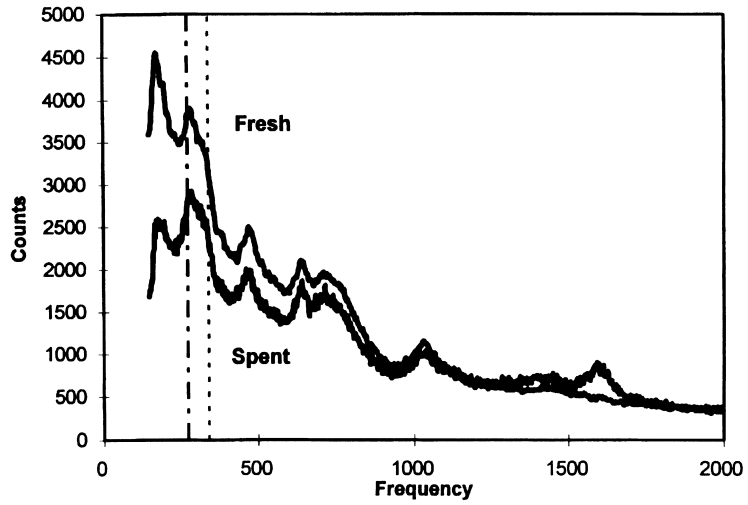

Fig. 9. UV–Raman spectra of fresh and deactivated sulfated zirconia catalysts {SZr/Al (600)}.

This is consistent with the UV–Raman pattern (Fig. 8). The 340/274 and 470/274 intensity ratios are 0.8 and 0.6, respectively. This suggests the surface crystal phase of SZr (600)/Al is tetragonal in nature. A broad sulfate band at 1031 cm^{-1} was observed. In comparison to the highly sulfated sample, this band was shifted to a lower frequency, indicating an increased covalency of the sulfate groups and suggests higher acid strength [32].

When SZr was stabilized with an alumina, a distinct monoclinic phase could not be detected in the UV–Raman spectra. The Raman band at 274 cm^{-1} clearly indicates the presence of tetragonal zirconia. Alumina appears to stabilize the active tetragonal phase of zirconia. Thermodynamic calculations made by Garvie et al. [14,15,33] indicate surface and strain energy effects determine the final crystal phase. Below a critical crystallite size, tetragonal zirconia is favored. As the size increases, monoclinic phase becomes the preferred crystal structure. Alumina may help prevent large crystallites from forming, thereby stabilizing the meta-stable tetragonal phase.

3.8. UV–Raman spectra of deactivated catalysts

Although the SZr catalyst showed good initial activity, quick deactivation prevents it from being used commercially. Catalyst deactivation can be associated with any of the following: a change in crystal structure, a change in sulfur oxidation state, or from hydrocarbon deposits. Fresh, spent, and regenerated SZr/Al (600) samples were characterized by UV–Raman spectroscopy to determine if a change in the surface zirconia phase could account for the catalyst deactivation (Fig. 9). All three spectra displayed a strong 274 cm^{-1} band, indicating tetragonal phase was present in the fresh and deactivated samples. The 340/274 and 470/274 intensity ratios are 0.8 and 0.6 for the fresh catalyst, and 0.7 and 0.6 for the deactivated samples. This indicates zirconium does not undergo a surface phase transformation as the catalyst deactivates.

Spent SZr/Al (600) contained 2.1 wt.% carbon and displayed a Raman band at 1620 cm^{-1}, which is assigned to deposited hydrocarbon fragments. Infrared studies indicate aromatic species are only formed after treating the spent catalyst at temperatures >300°C. Alkylation runs performed in this study were conducted at 28°C, therefore aromatic compounds were not expected to form. In addition, a similar band was observed after treating SZr (600) with isobutane at room temperature. As suggested by other researches, deactivation is most likely caused by the accumulation of hydrocarbon fragments on the catalyst surface [1,2]. Eventually, hydrocarbon fragments cover the active sites, thereby poisoning the activity. Regeneration of the catalyst in air at 600°C for 2 h completely removes the hydrocarbon fragments and restores the catalytic activity. SZr/Al (600) underwent several regeneration cycles without any apparent loss in activity.

4. Conclusions

Results presented in this study are consistent with the tetragonal zirconia phase being more active than the monoclinic phase. Catalyst formulations containing either silica or alumina displayed prolonged activity. Additives appear to limit the formation of large zirconia crystallites, thereby stabilizing the tetragonal phase. UV–Raman spectroscopy indicates active catalysts contain a well-defined tetragonal phase on their surface. While distinct tetragonal reflections were absent on samples displaying poor catalytic activity.

The most active catalyst system for either hexane cracking or isoparaffin alkylation was obtained when sulfur loading levels approached monolayer coverage (4 atoms/nm^2). This corresponds to a surface coverage of one sulfur atom for every two zirconium atoms. The catalyst Brønsted acidity is also maximized at sulfur loading level of 4 atoms/nm^2.

UV–Raman spectra of fresh and deactivated catalysts indicate the zirconium surface structure did change during the alkylation reaction. Catalyst deactivation is probably the result of hydrocarbon fragments building up on the surface and blocking access to the active sites.

References

[1] X. Song, A. Sayari, Catal. Rev. 38(3) (1996) 329.
[2] B.H. Davis, R. Keogh, R. Srinivasan, Catal. Today 20 (1994) 219.
[3] K. Arata, Adv. Catal. 37 (1990) 165.
[4] T. Yamaguchi, Appl. Catal. 61 (1990) 1.
[5] K. Tanabe, H. Hattor, T. Yamaguchi, Crit. Rev. 1 (1990) 1.
[6] M. Misino, T. Okuhara, Chemtech (1993) 23.
[7] T. Jin, T. Yamaguchi, K. Tanabe, J. Phys. Chem. 90 (1986) 4794.
[8] G. Yalaris, R.B. Larson, J.M. Kobe, M.R. Gonzales, K.B. Fogash, J.A. Dumesic, J. Catal. 158 (1996) 336.
[9] A.M. Yousef, S.E. Samra, H.M. Abou-El Nador, E.A. El-Sharkawy, Bull Soc. Chim. Fr. 128 (1991) 604.
[10] R. Srinivasan, C.R. Hubbard, O.B. Cavin, B. Davis, Materials 5 (1993) 27.
[11] A. Clearfield, Inorg. Chem. 3 (1964) 146.
[12] J.A. Schwartz, Catal. Today 15 (1992) 395.
[13] A. Corma, V. Fornes, M.I. Juan-Rajadell, J.M. Lopez-Nieto, Appl. Catal. A. 116 (1994) 151.
[14] R.C. Garvie, M.F. Goss, J. Mater. Sci. 21 (1986) 1253.
[15] R.C. Garvie, J. Phys. Chem. 82 (1978) 218.
[16] P.D.L. Mercera, J.G. Van Ommen, E.B.M. Doesburg, A.J. Burggraaf, J.R.H. Ross, Appl. Catal. 57 (1990) 127.
[17] C.J. Norman, P.A. Goulding, I. McAlpine, Catal. Today 20 (1994) 313.
[18] T. Katapla, J.A. Dumesic, J. Catal. 112 (1988) 66.
[19] S. Alerasool, P.K. Doolin, J.F. Hoffman, Effect of matrix acidity on resid cracking activity of FCC catalysts, in: Mario L. Occelli, Paul O'Connor (Eds.), Fluid Cracking Catalysts, Marcel Dekker, 1998, pp. 99–110.
[20] B. Umansky, J. Engelhardt, W.K. Hall, J. Catal. 127 (1990) 128.

[21] D. Chen, S. Sharma, N. Cardona-Martinez, J.A. Dumesic, V.A. Bell, G.D. Hodge, R.J. Madon, J. Catal. 136 (1988) 392.
[22] J.J. Venter, M.A. Vannice, Appl. Spectry 42 (1988) 1096.
[23] C. Li, P.C. Stair, Catal. Lett. 36 (1996) 119.
[24] P.C. Stair, C. Li, J. Vac. Sci. Technol., A. 15 (1998) 1679.
[25] C. Li, P.C. Stair, Stud. Surf. Sci. Catal. 101 (1996) 881.
[26] M.T. Tran, N.S. Gnep, G. Szabo, M. Guisnet, Appl. Catal. A 171 (1998) 207.
[27] C.R. Vera, J.M. Parera, J. Catal. 165 (1997) 254.
[28] R. Srinivasan, D. Taulbee, B. Davis, Catal. Lett. 9 (1991) 1.
[29] M. Hino, S. Kobayashi, K. Arata, J. Am. Chem. Soc. 101 (1979) 6439.
[30] M. Hino, K. Arata, J. Chem. Soc. Chem. Commun. (1980) 851.
[31] C. Morterra, G. Cerrato, F. Pinna, M. Signoretto, J. Catal. 157 (1995) 109.
[32] C. Morterra, G. Cerrato, M. Signoretto, Catal. Lett. 41 (1996) 101.
[33] R.C. Garvie, J. Phys. Chem. 69 (1965) 1238.